مجلة كلية التربية الاساسية
كلية التربية الاساسية – الجامعة المستنصرية
P- ISSN: 3007-3650 E- ISSN: 2706-8536
Journal of the College of Basic Education Vol.32 (No.137) 2026, pp.1110-1130

Phytosynthesis And Structural–Optical Study Of Ag/Ag_2O Nanoparticles Using Mixture Of Leaves And Immature Fruits Extract Of Iraqi Christ's Thorn

(1) **Sundus Hadi Merza**
Department of Chemistry, College of Education for Pure Science / Ibn Al-Haitham, University of Baghdad, Iraq

1 sundus.h.m@ihcoedu.uobaghdad.edu.iq

Abstract:
This study reports a novel green and straightforward method for synthesizing silver/silver oxide nanoparticles (Ag /Ag_2O NPs) using a mixture of immature fruits and leaves extract of Iraqi christ's thorn (IF-LCT). Synthesis of Ag /Ag_2O NPs was verified by visual observation in which the $AgNO_3$ solution turned to a brown-colored solution. The Ag/Ag_2O NPs caused surface plasmon resonance (SPR) at 440 nm. Subsequent characterization was done by X-ray diffraction (XRD), ultraviolet-visible (UV-Vis), Fourier transform infrared (FTIR), field emission scanning electron microscope (FE-SEM) and energy dispersion X-ray spectroscopy (EDXS). The average crystallite size of the Ag/Ag_2O NPs as assessed by XRD was determined to be 15.89 nm. All the other parameters approved synthesizes Ag/Ag_2O NPs with a high surface area to volume ratio, high atomic packing factor (APF) and notably high specific surface area. FE-SEM analysis shown the silver NPs appeared as agglomerated spherical and quasi-spherical structure with average particles size equal to 21.65 nm. EDXS evidenced that nanoparticles contain silver and oxygen. The finest conditions for phytosynthesis of Ag NPs using aqueous extract to silver nitrate (1:10) ratio at 25 °C. The direct band gap was 2.96 eV. FTIR exhibited the particular stretch of bands of the synthesized Ag/Ag_2O NPs. The aforementioned outcomes demonstrated that the Ag/Ag_2O NPs were effectively prepared using IF-LCT extract.

Key words: specific surface area, atomic packing factor, Scherrer equation, Ag NPs, face centered cubic.

Introduction:

Ziziphus spina-Christi is a non-deciduous tree from the Rhamnaceae family growing in a tropical and subtropical Zone in Africa, southern and western Asia including Iraq (Norouzi et al., 2017) (Ziziphus et al., 2026). Ziziphus is a global genus comprising 58 recognized species (El Maaiden et al., 2020). The genus Ziziphus is one of the most important perennial thorny species that is fast-growing, drought-tolerant, and evergreen. Ziziphus spina-Christi is also called Nabag, Sidr and Christ's thorn (CT) (Ziziphus et al., 2026). CT trees have high ability to withstand drought conditions and their wide adaptation to different types of soil (Al-Zaydi & Al-Jibouri, 2025). Additionally, CT offers economic advantages in the food and pharmaceutical sectors. CT has long been utilized in traditional medicine and therapeutic applications, in addition to its disinfecting qualities. CT trees also exhibit soothing effect, anti-inflammatory, anticancer, antimicrobial, and antioxidant (Mohammed & Al-Brahim, 2014) due to presence of various bioactive substances, including flavonoids, tannins, carbohydrates, alkaloids, vitamins, saponins and christinin (Saied et al., 2008) (Asgarpanah, 2012). The phytochemicals are available, ecofriendly, and ordinarily non-toxic. As a result, green synthesis has emerged as one of the most advantageous approaches as it avoids toxic and harmful reducing agents (Gevorgyan et al., 2022). Plant-based phytochemicals are involved in mechanism of reduction and capping process to prepare silver nanoparticles. Noble silver and its oxide particularly, Ag_2O play a crucial role in nanomaterial science owing to its exceptional physical and chemical properties and thus its application (Jemal et al., 2017). Numerous studies have utilized various parts of the CT plant such as root, leaves, fruits, seeds and bark as reducing, capping and stabling agents to prepared Ag NPs (Al-Bahrani et al., 2018; El-Ansary et al., 2018; Faraj et al., 2023; Mostafa et al., 2020; Yagoub et al., 2021). To the best of our knowledge, no previous studies have reported the use of a blend extract of immature fruits and leaves of Iraqi Christi Thorn (IF-LCT). Therefore, the present study provides an environmentally friendly, economical and efficient method for synthesis

مجلة كلية التربية الاساسية
كلية التربية الاساسية – الجامعة المستنصرية
P- ISSN: 3007-3650 E- ISSN: 2706-8536
Journal of the College of Basic Education Vol.32 (No.137) 2026, pp.1110-1130

Ag NPs utilizing a non-toxic, low-cost blended extract of IF-LCT. The structural, and optical properties of the synthesized silver nanoparticles were characterized using XRD, FTIR, UV-Vis, TGA, EDXS and FESEM analyses.

Materials and method

Preparation of immature Christ's Thorn fruits and leaves extract and phytosynthesis of silver nanoparticles

Immature fruits and leaves of Christ's Thorn (IF-LCT) were collected from a private garden in Baghdad in November [Figure 1a and b]. Prior to air drying, the plant materials were thoroughly washed with distilled water. After drying, the seedless fruits and leaves were ground into a fine powder using an electric grinder. The resulting powder was stored in sealed and labeled glass container. Then, approximately 5 g of each immature fruit and leaf powder were mixed with 100 mL of distilled water and continuously stirred at 40 °C for 20 minutes. A centrifuge was used to separate the mixture. Prior to use, the viscous supernatant of IF-LCT was collected and stored at 4 °C. For the synthesis of silver nanoparticles (Ag NPs), 1ml of IF-LCT extract was added to 10 mL of silver nitrate solution at different concentrations of 0.1, 0.01, 1 $\times 10^{-3}$, and 5 $\times 10^{-3}$ M. The color change of the solution indicated the formation of Ag NPs [Figure 1c]. Finally, Ag NPs were collected by centrifugation and washed with distilled water to eliminate excess silver ions [Figure 1d].

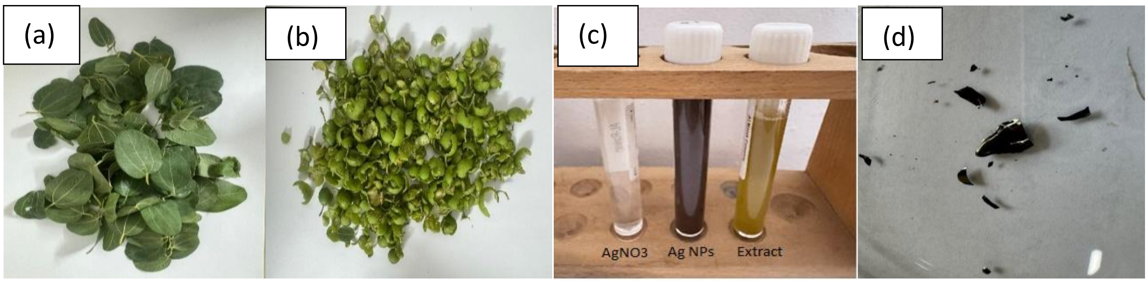

Figure 1: Images of Christ's Thorn (a) leaves (b) seedless fruits (c) $AgNO_3$ solution, Ag NPs solution and IF-LCT extract (d) Ag NPs.

Characterization of Ag NPs

The powder of the resultant Ag NPs was analyzed using X-Ray Diffractometer (XRD/6000 from SHIMADZU-Japan). To detect the effective functional groups, the spectrophotometer of Fourier transforms infrared (FTIR) type (Shimadzu, 8400 s, Japan) was used. The optical properties of Ag NPs solution were studied using spectrophotometer, double beam, (v-650, Japan). The morphology and elemental composition were investigated by field emission scanning electron microscopy (FESEM) and energy dispersive X-Ray spectroscopy (EDXS) from (MIRA3 TESCAN, FRENCH).

Result and Discussion

Crystal structure analysis of Ag NPs

XRD analysis was used to verify the synthesis, crystalline nature, and size of Phyto-Ag NPs. As seen in Figure 2, the XRD pattern of the Ag NPs produced by IF-LCT was recorded at 2θ angles between 20 and 80 degrees. The XRD spectrum of the Ag NPs shows the main Bragg diffraction peaks with its miller index around 38.07 (111), 44.24 (200), 64.43 (220), and 77.35 (311) respectively, reflection planes of the face-centered cubic (FCC) structure of silver. These diffraction peaks showed strong agreement with the Joint Committee on Powder Diffraction Standards (JCPDS) card no. 04-0783(Wei et al., 2020). Additional peaks attributed to cubic Ag_2O were also detected at 32.20 (relative intensity 100%), 38.07 (overlaps with Ag), 54.80, and 67.35 (Pham et al., 2015). The existence of organic molecules in IF-LCT may be indicated by the additional peaks detected at 27.76, 46.20 and 57.43 (marked with asterisk symbol) (Tanwar & Joseph, 2025). The capping and reducing phytochemicals in the IF-LCT stabilize the produced nanoparticles, giving the Ag NPs their crystalline character (sharp peaks of Bragg angles) (Rautela et al., 2019) (Kumar et al., 2012).

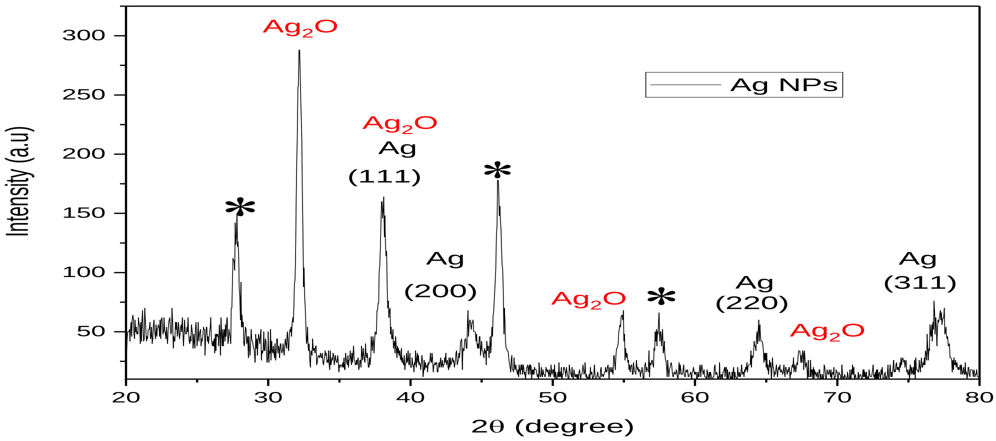

Figure 2: XRD diffractogram of Ag/Ag_2O NPs.

The Scherrer equation was employed to determine the crystal size (D) of Ag NPs, D = (K λ) / (β cos θ) (Merza, 2025). The Cu K_α X-ray wavelength is represented by λ which equal to 0.1540 nm, the full width at half maximum (FWHM) intensity of the X-ray peak by β (rad), the K shape factor constant (0.94), and the reference peak width is indicated by the angle θ. The average crystal size of AgNPs was determined to be 16.57 nm (Roopan et al., 2013)(Fayyadh & Jaduaa Alzubaidy, 2021). The distance between the atomic planes (d) is calculated from Bragg's equation $n\,\lambda = 2d\sin\theta$ where the first order reflection is denoted by n. The d values and XRD data were summarized in Table 1.

Table 1:The d values and XRD data of Ag NPs

2θ	FWHM (rad)	Crystal size D (nm)	d spacing (Cal.)	d spacing (Ins.)	d JCPDS (04-0783)	(a)	SSA (m^2/g)
38.0720	0.0094	16.2776	0.2364	0.2361	0.2362	0.4089	35.1385
44.2428	0.0125	12.5160	0.2047	0.2045	0.2036	0.4090	45.6993
64.4300	0.0100	17.0514	0.1450	0.1444	0.1432	0.4084	33.5439
77.3592	0.0104	17.7408	0.1233	0.1232	0.1200	0.4086	32.2404
	Average	15.89				0.4086	
Cal: calculation Ins: instrument a: Lattice parameter							

مجلة كلية التربية الاساسية
كلية التربية الاساسية – الجامعة المستنصرية
P- ISSN: 3007-3650 E- ISSN: 2706-8536
Journal of the College of Basic Education Vol.32 (No.137) 2026, pp.1110-1130

The crystal axes of the unit cell, lattice parameter (a) of face -centered cubic (FCC) crystal structure of Ag NPs was calculated using the following formula $\frac{1}{d^2} = \frac{h^2+k^2+l^2}{a^2}$ where h, k, l is the Miller indices. The values of (a) tabulated in Table 1. The average (a) values of Ag and Ag_2O calculated to be 0.4086 and 0.4717 respectively which are well matched with lattice parameter of Ag NPs (JCPDS 04-0783) and Ag_2O (JCPDS 41-1104) (Dharavath et al., 2025)(Pham et al., 2015). This finding further verified that the synthesized silver nanoparticles existed in two phases: Ag and Ag_2 O.
The atomic radius (r) of the prepared Ag NPs was calculated using the formula $r = \frac{a\sqrt{2}}{4}$, yielding a value of 0.1444 nm (Ali et al., 2023). The atomic packing factor (APF) was determined to be 0.74, by substituting the volume of unit cell of FCC $V_{uc} = a^3 = \left(\frac{4r}{\sqrt{2}}\right)^3 = 22.6274\, r^3$ and volume of unit cell $V_{Ag} = \frac{4\pi r^3}{3}$ together with the number of atoms N_a= 4 in the following equation $APF = \frac{N_a \times V_{Ag}}{V_{uc}}$, indicating that the atoms of Ag are closely packed in a unit cell (maximum density) which improved the structural stability and mechanical strength of the Ag NPs prepared from IF-LCT. Additionally, the surface area-to-volume ratio was also computed for IF-LCT-Ag NPs. The Ag NPs surface area, $S_{Ag} = 4\pi r^2$ and particles volume $V_{Ag} = \frac{4}{3}\,\pi r^2$ resulted in a ratio of 3×10^9. This figure is significantly boosting the efficiency and reactivity of Ag NPs particularly, in antimicrobial application and catalytic reaction (Fahim et al., 2024). Furthermore, the specific surface area (SSA) of the Ag NPs was evaluated using the relation ($\frac{6 \times 1000}{D \times \rho}$) where D and ρ are the size of AgNPs (nm) and the density of silver (10.94×10^6 g. m^{-3}). The SSA values (m^2/g) [Table 1] increased as the particles size decreased. The value of SSA was found to be larger than SSA calculated for Pathor Kuchi leaf extract/AgNPs (Theivasanthi & Alagar, 2012).

FT-IR Spectral analysis

FTIR analysis was carried out to recognize the potential functional groups of the phyto-AgNPs. Ziziphus Spina-Christi is mainly composed of alkaloids, flavonoids and saponins (Dahiru et al., 2025). Hence, the characteristic bands of these phytochemicals were detected by FTIR spectrum Figure 3.

FTIR spectrum of IF-LCT-Ag/Ag_2O showed a broad band in the range larger than 3500 cm^{-1} may be attributed to the stretching vibration of N-H groups, phenolic and alcohols compounds. The absorption peak which resembled the C-H symmetrical/ a symmetrical stretching frequency of CH_3, CH_2 and CH_3-O groups emerged at 2914 cm^{-1} and 2842 cm^{-1}, these groups play significant role in activated the functional groups through donated electron density (Maheshwaran et al., 2020). Furthermore, the band at 1600 cm^{-1} and 1502 cm^{-1} assigned to C=C stretching vibration of aromatic ring and/or conjugated alkene. The peak at 1871 cm^{-1} attributed to the stretching of C-H holding aromatic groups (Venkatachalam et al., 2015). In the 1500 to 400 cm^{-1} region, the peak at 969 cm^{-1} is indicative of C-H group out of plane bending. The bending vibration of C-H moieties was observed at 1431 cm^{-1}. The stretching vibration of phenolic groups C-O is responsible for the peak at 1193 cm^{-1}. The stretching vibration of C-N aromatic amine appeared at 1342 cm^{-1} (Coates, 2000). Finally, the weak peaks in the 435 cm^{-1} and 811 cm^{-1} are associated to Ag-O bond (Kokila et al., 2015) (Rani et al., 2020). All the band vibration mentioned previously may be result of functional groups that play a role in capping Ag NPs and reduction silver ions.

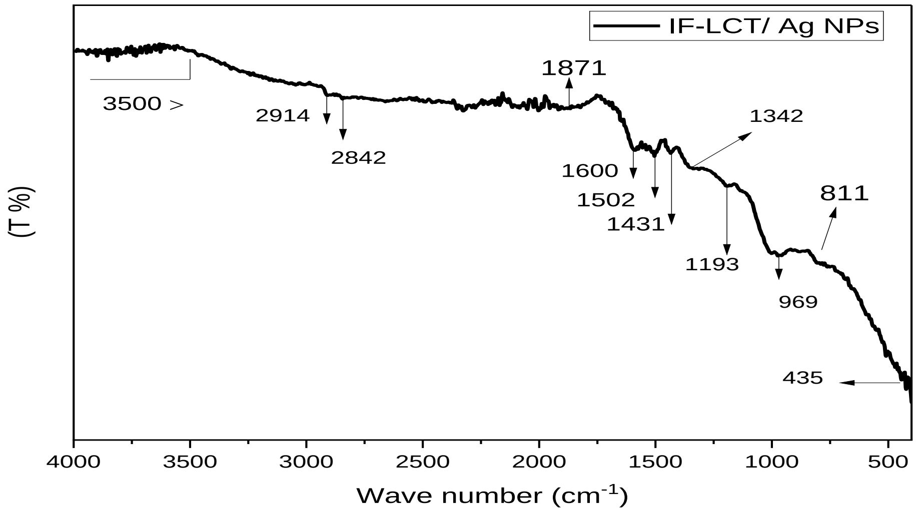

Figure 3: FTIR spectrum of IF-LCT-Ag NPs

Band gap analysis of Ag NPs

To evaluate the synthesis process, investigate the electronic transitions of Ag NPs and determine the optimal silver nitrate concentration, UV-Visible analysis was carried out. Figure 4a present the UV-Visible spectra of the colloidal silver nanoparticles recorded at different concentration ranging 0.1–0.001 M and 1:10 volume ratio of IF-LCT to silver nitrate solution. At concentration of 0.1M silver nitrate, a broad absorption spectrum with maximum at λ_{max} = 498 nm was observed. As the silver nitrate concentration decrease to 0.001 M the λ_{max} shifted to shorter wavelengths reaching, 440 nm (Pawar et al., 2016). The gradual constriction in the peaks accompanied by a blue shift of around 49 nm indicates a reduction in the average particle size of silver nanoparticles. The presence of an influential absorption peak is characteristic of nanoscale metal particles when contrasted with bulk metal spectra (Aziz et al., 2019). According to Mie's theory the appearance of a single surface plasmon resonance (SPR) band is characteristic of spherical or quasi spherical nanoparticles and reflects increased symmetry and uniformity in particle size distribution (Pal et al., 2007).The SPR peak finding is consistent with the following studies (Masoud E. A & A. Al-

Marrani, 2016) (Mostafa et al., 2020) (Ali et al., 2023). The synthesis of Ag NPs using different volume ratios of IF-LCT to 0.001 M of silver nitrate solution was also carried out at room temperature [Figure 4b]. The maximum absorption peak appeared at 440, 470, 480 and 488 nm at,1:10, 10:5, 5:10 and 3:5 ratios respectively. The SPR bands exhibited a shift toward a higher wavelength and became wider with lower intensities as compared to the 1:10 ratio suggesting possible destabilization and increased aggregation of nanoparticle. This is because the shape and position of plasmon absorption of silver nanoclusters are powerfully dependent on particle size and surface-adsorbed species (Pal et al., 2007). Therefore, the 0.001 M at 1: 10 ratio is the optimal concentration for the formation of Ag NPs.

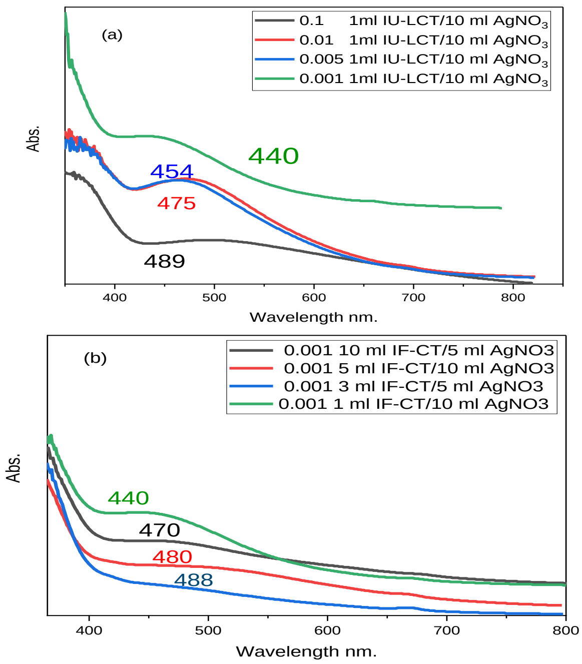

Figure 4: UV-Visible spectra of Ag NPs at different concentration with 1:10 IF-LCT to $AgNO_3$ ratio (a) and at 0.001 M with different volume ratios IF-LCT to $AgNO_3$ (b).

مجلة كلية التربية الاساسية
كلية التربية الاساسية – الجامعة المستنصرية
P- ISSN: 3007-3650 E- ISSN: 2706-8536
Journal of the College of Basic Education Vol.32 (No.137) 2026, pp.1110-1130

The energy bandgap (E_g) of the colloidal Ag/Ag_2O was calculated using Tauc's equation $(\alpha h\nu)^n = B(h\nu - E_g)$. The bandgap was estimated by extrapolating a straight line on the energy axis. The definition of the absorption coefficient α is $\alpha = 2.302 \times A$ where A is the measured absorbance and B is proportionality constant. The energy of photon is given by $h\nu = \frac{hc}{\lambda} = \frac{1240\ ev}{\lambda\ (nm)}$ where h, c and λ are Planck's constant, the speed of light and the wave length respectively. The electronic transition mode whether direct or indirect can be diagnosed from power factor n. The energy gap (E_g) is obtained by plotting $(\alpha h\nu)^n$ versus energy. In this research, n = 2 provided the best fit of the experimental data. As shown in Figure the estimated band gap of silver NPs solution was 2.96 eV. This value is higher than previously reported value likely, due to particle size effect and quantum confinement (Parmar et al., 2020)
(Shameran et al., 2019).

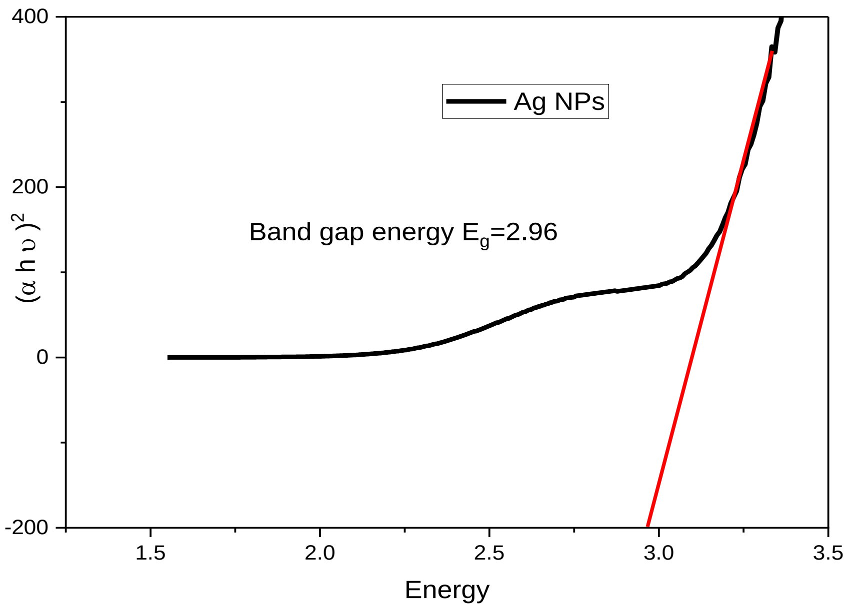

Figure 5: Band gap energy of colloidal Ag/Ag_2O NPs

Morphology analysis

مجلة كلية التربية الاساسية
كلية التربية الاساسية – الجامعة المستنصرية
P- ISSN: 3007-3650 E- ISSN: 2706-8536
Journal of the College of Basic Education Vol.32 (No.137) 2026, pp.1110-1130

The analytical techniques field emission scanning electron microscopy (FE-SEM) and energy-dispersive X-ray spectroscopy (EDXS) were used to visualize the morphology and determine the elements that attributing the nanostructure of Ag/Ag_2O NPs respectively. Figure 6a illustrates the FE-SEM of fabricated Ag/Ag_2O NPs. The Ag/Ag_2O NPs were quasi spherical particles with dense clusters. Furthermore, the histogram [Figure 6b] showed distribution of particles size with an average size of 21.65 nm larger than those estimated by the Debye-Scherrer equation due to agglomeration.

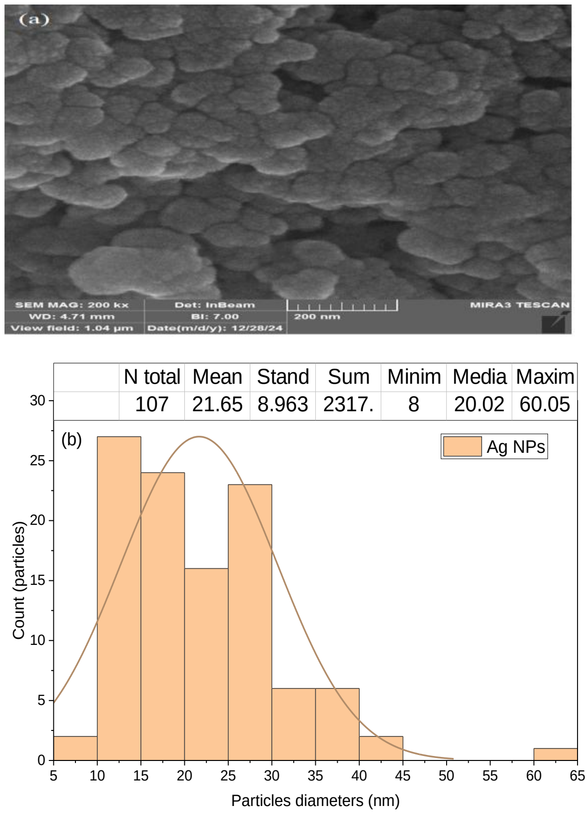

Figure 6: FE-SEM image of IF-LCT -Ag/Ag_2O NPs (a) and histogram of average particle size by Image J (b).

EDX analysis [Figure 7] was used to approve the preparation of Ag/Ag_2O NPs. The x– ray emission peaks confirm the presence of two signals of

Ag (Ag L_α and Ag L_β) with weak signal of O (O K_α). The EDX spectrum confirms the presence of silver through a characteristic peak at around 3 keV (Ag Lα), along with a weak oxygen signal at 0.5 keV indicating the formation of Ag/Ag_2O nanoparticles. Besides, Cl signals (Cl K_α) and (Cl K_β) were observed, arising from X-ray emission of phytochemicals present in the IF-LCT. Comparable findings were also documented by Ali Abdullah Fayyadh et al (Fayyadh & Jaduaa Alzubaidy, 2021).

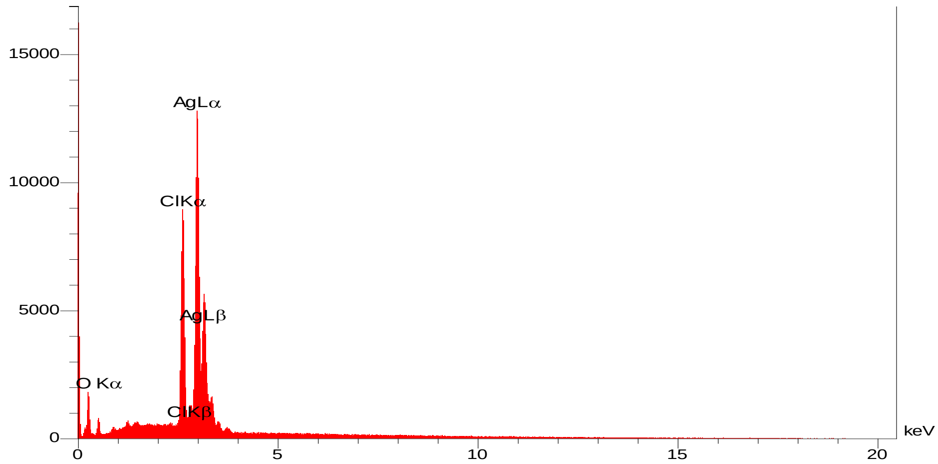

Figure 7: EDX spectrum of IF-LCT- Ag/Ag_2O

Thermogravimetric (TG) and derivative thermogravimetry (DTG) analysis

The thermogravimetric and derivative thermogravimetry (TG/DTG) diagrams of phyto-AgNPs is shown in Figure 8. DTG and TGA was accomplished to figure out the thermal stability and existence of oxygen functionality on the IF-LCT/ AgNPs. TGA thermogram of the AgNPs [Figure 8a] displayed four weight loss of steps. The first and second decomposition steps occurs between the temperatures 25–135°C and 135–210 °C with weight loss (3.3% and 4.42%) respectively, representing the removal of moisture and volatile moieties holding IF-LCT /AgNPs. The third step was detected from 210 °C - 315 °C with 9.37% weight loss, ascribed to the breakdown of the low molecular weight phytochemical coating of Ag NPs such as alcoholic, alkaloids, flavonoids and saponins compounds. This outcome is compatible with the FTIR analysis. The final step is attributed to the decomposition of oxygen residue at elevated temperatures between 315 °C and 835 °C with a weight loss of 20.67% (Gharari et al., 2022). The most noticeable weight loss points were revealed by derivative thermogravimetry (DTG) [Figure 8b]. The TGA measurement showed that the volatile and phytochemicals were adhered to the IF-LCT-Ag NPs.

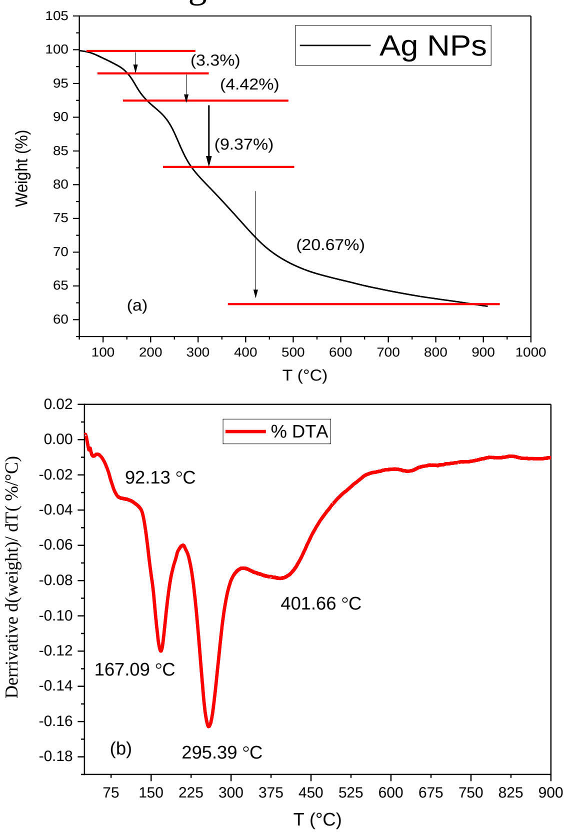

Figure 8: TGA(a) and DTG (b) of IF-LCT-Ag/Ag_2O NPs.

Conclusions

In this study, silver NPs were synthesized using blend of immature Christ's Thorn fruits and leaves as potential reducer, capping and stabilizer phytochemicals. The successful synthesis of Ag/Ag_2O NPs was confirmed by XRD, FTIR, UV–vis, FESEM, EDXS, and TGA analyses. The XRD analysis reveals the formation of two phases of Ag NPs and Ag_2O NPs corresponding to a face-centered cubic (FCC) and cubic structure with average particle size of 15.89 nm. The FTIR spectrum exposes the distinctive peaks for phytoconstituents as well as Ag–O stretching vibration. FE-SEM analysis demonstrates that the particles aggregate in spherical and quasi- spherical shapes with an average particle size of 21.65 nm larger than those estimated by the Debye-Scherrer equation due to agglomeration. EDX analysis confirms that the IF-LCT-Ag/Ag_2O NPs exhibit a strong absorption peak at 3 KeV and a weak peak approximately at 0.5 KeV corresponding to silver nanocrystals and oxygen, respectively. The peak of surface plasmon resonance (SPR) in UV-Vis region displayed a blue shift at 440 nm with energy bandgap at 2.96 eV. The specific surface area (SSA) for the dominant peak (111) plane is 35.1385 m^2/g and atomic packing fraction (APF) is found 0.74. Finally, the surface area to volume ratio is significantly high. This study produced a rapid, simple, and environmentally friendly method for the phytosynthesis of Ag/Ag_2O NPs by mixture of immature fruits and leaves Christ's Thorn extract.

Acknowledgment

The authors are grateful for the support from the Department of Chemistry / College of Pure Science (Ibn Al-Haitham) / University of Baghdad.

Authors' Declaration

The authors declare that there are no conflicts of interest regarding the publication of this manuscript.

References

Al-Bahrani, R. M., Majeed, S. M. A., Owaid, M. N., Mohammed, A. B., & Rheem, D. A. (2018). Phyto-fabrication, characteristics and anticandidal effects of silver nanoparticles from leaves of Ziziphus mauritiana lam. *Acta Pharmaceutica Sciencia*, *56*(3), 85–92. https://doi.org/10.23893/1307-2080.APS.05620

Al-Zaydi, R. A. Y., & Al-Jibouri, A. I. J. (2025). Diagonal Growth Curve for (Ziziphus Spina Christi) Growing in Governorate Anbar. *Iraqi Journal of Agricultural Sciences*, *56*(2), 850–857. https://doi.org/10.36103/bw4j0y71

Ali, M. H., Azad, M. A. K., Khan, K. A., Rahman, M. O., Chakma, U., & Kumer, A. (2023). Analysis of Crystallographic Structures and Properties of Silver Nanoparticles Synthesized Using PKL Extract and Nanoscale Characterization Techniques. *ACS Omega*, *8*(31), 28133–28142. https://doi.org/10.1021/acsomega.3c01261

Asgarpanah, J. (2012). Phytochemistry and pharmacologic properties of Ziziphus spina christi (L.) Willd. *African Journal of Pharmacy and Pharmacology*, *6*(31), 2332–2339. https://doi.org/10.5897/ajpp12.509

Aziz, S. B., Hussein, G., Brza, M. A., Mohammed, S. J., Abdulwahid, R. T., Saeed, S. R., & Hassanzadeh, A. (2019). Fabrication of interconnected plasmonic spherical silver nanoparticles with enhanced localized surface plasmon resonance (Lspr) peaks using quince leaf extract solution. *Nanomaterials*, *9*(11), 1–15. https://doi.org/10.3390/nano9111557

Coates, J. (2000). Interpretation of Infrared Spectra, A Practical Approach. *Encyclopedia of Analytical Chemistry*, 1–23. https://doi.org/10.1002/9780470027318.a5606

Dahiru, M. M., Hauwa, A. Y., Zainab, M., Pius, P., & Yakubu, N. D. (2025). Fourier-transform Infrared (FTIR) Characterization and Radical Scavenging Activity Ziziphus spina-christi (Rhamnaceae) Rootbark Fractions. *Majalah Obat Tradisional*, *30*(2), 179–189. https://doi.org/10.22146/mot.95278

Dharavath, S. B., Maduru, N., Porika, M., Chirumamilla, P., Veera, S., Ponnam, N., & Taduri, S. (2025). Green synthesis of silver nanoparticles using Nothapodytes foetida leaf extract: Optical, antibacterial and anticancer activities. *Next Nanotechnology*, *7*(March), 1–9.

https://doi.org/10.1016/j.nxnano.2025.100162
El-Ansary, A., Warsy, A., Daghestani, M., Merghani, N. M., Al-Dbass, A., Bukhari, W., Al-Ojayan, B., Ibrahim, E. M., Al-Qahtani, A. M., & Bhat, R. S. (2018). Characterization, antibacterial, and neurotoxic effect of Green synthesized nanosilver using Ziziphus spina Christi aqueous leaf extract collected from Riyadh, Saudi Arabia. *Materials Research Express*, *5*(2), 1–11. https://doi.org/10.1088/2053-1591/aaaf5f
El Maaiden, E., El Kharrassi, Y., Qarah, N. A. S., Essamadi, A. K., Moustaid, K., & Nasser, B. (2020). Genus Ziziphus: A comprehensive review on ethnopharmacological, phytochemical and pharmacological properties. In *Journal of Ethnopharmacology* (Vol. 259). Elsevier B.V. https://doi.org/10.1016/j.jep.2020.112950
Fahim, M., Shahzaib, A., Nishat, N., Jahan, A., Bhat, T. A., & Inam, A. (2024). Green synthesis of silver nanoparticles: A comprehensive review of methods, influencing factors, and applications. *JCIS Open*, *16*(September), 1–23. https://doi.org/10.1016/j.jciso.2024.100125
Faraj, M., Faraj, A., & Erhayem, M. (2023). Eco-Friendly Synthesis of Silver Nanoparticles Using Aqueous Extract of Ziziphus Spina-Christi Seeds: Characterization and Stability. *Journal of Pure & Applied Sciences*, *22*(2), 40–45. https://doi.org/10.51984/jopas.v22i2.2676
Fayyadh, A. A., & Jaduaa Alzubaidy, M. H. (2021). Green-synthesis of Ag2O nanoparticles for antimicrobial assays. *Journal of the Mechanical Behavior of Materials*, *30*(1), 228–236. https://doi.org/10.1515/jmbm-2021-0024
Gevorgyan, S., Schubert, R., Falke, S., Lorenzen, K., Trchounian, K., & Betzel, C. (2022). Structural characterization and antibacterial activity of silver nanoparticles synthesized using a low-molecular-weight Royal Jelly extract. *Scientific Reports*, *12*(1), 1–12. https://doi.org/10.1038/s41598-022-17929-y
Gharari, Z., Hanachi, P., & Walker, T. R. (2022). Green synthesized Ag-nanoparticles using Scutellaria multicaulis stem extract and their selective cytotoxicity against breast cancer. *Analytical Biochemistry*, *653*(2022), 1–

14. https://doi.org/10.1016/j.ab.2022.114786
Jemal, K., Sandeep, B. V., & Pola, S. (2017). Synthesis, Characterization, and Evaluation of the Antibacterial Activity of Allophylus serratus Leaf and Leaf Derived Callus Extracts Mediated Silver Nanoparticles. *Journal of Nanomaterials*, *2017*, 1–11. https://doi.org/10.1155/2017/4213275
Kokila, T., Ramesh, P. S., & Geetha, D. (2015). Biosynthesis of silver nanoparticles from Cavendish banana peel extract and its antibacterial and free radical scavenging assay: a novel biological approach. *Applied Nanoscience (Switzerland)*, *5*(8), 911–920. https://doi.org/10.1007/s13204-015-0401-2
Kumar, R., Roopan, S. M., Prabhakarn, A., Khanna, V. G., & Chakroborty, S. (2012). Agricultural waste Annona squamosa peel extract: Biosynthesis of silver nanoparticles. *Spectrochimica Acta - Part A: Molecular and Biomolecular Spectroscopy*, *90*(2012), 173–176. https://doi.org/10.1016/j.saa.2012.01.029
Maheshwaran, G., Nivedhitha Bharathi, A., Malai Selvi, M., Krishna Kumar, M., Mohan Kumar, R., & Sudhahar, S. (2020). Green synthesis of Silver oxide nanoparticles using Zephyranthes Rosea flower extract and evaluation of biological activities. *Journal of Environmental Chemical Engineering*, *8*(5), 1–11. https://doi.org/10.1016/j.jece.2020.104137
Masoud E. A, .Al-Hajry M, & A. Al-Marrani. (2016). Antibacterial Activity of Silver Nanoparticles Synthesized by Sidr (Ziziphus spina-Christi) Leaf Extract against Pathogenic Bacteria. *International Journal of Current Microbiology and Applied Sciences*, *5*(4), 226–236. https://doi.org/10.20546/ijcmas.2016.504.028
Merza, S. H. (2025). Impact of defect- containing graphene oxide nanosheets on the structural, electrical, and die;ectrical characteristics of graphene oxide. *Bulletin of the Chemical Society of Ethiopia*, *39*(12), 2583–2592.
Mohammed, A. E., & Al-Brahim, J. S. (2014). Synthesis, characterization and evaluation of antimicrobial potency of silver nanoparticles using Ziziphus spina-christi L. leaf extract. *Journal of Pure and Applied*

Microbiology, *8*(5), 3903–3908.

Mostafa, M., AL-Emam, A., Sayed, M., AlAmri, S., ALGhamdil, H., SHati, A., ALrumman, S., & ALFaify, A. K. (2020). Silver nanoparticles from ziziphus spina-christi (l.) desf. fruits extract and their antimicrobial activity. *Bangladesh Journal of Botany*, *49*(4), 1127–1134. https://doi.org/10.3329/bjb.v49i4.52629

Norouzi, E., Erfani-moghadam, J., Fazeli, A., & Khadivi, A. (2017). Morphological variability within and among three species of Ziziphus genus using multivariate analysis. *Scientia Horticulturae*, *222*(2017), 180–186. https://doi.org/10.1016/j.scienta.2017.05.016

Pal, S., Tak, Y. K., & Song, J. M. (2007). Does the antibacterial activity of silver nanoparticles depend on the shape of the nanoparticle? A study of the gram-negative bacterium Escherichia coli. *Applied and Environmental Microbiology*, *73*(6), 1712–1720. https://doi.org/10.1128/AEM.02218-06

Parmar, A., Kapil, S., Sachar, S., & Sharma, S. (2020). Design of experiment based methodical optimization and green syntheses of hybrid patchouli oil coated silver nanoparticles for enhanced antibacterial activity. *Current Research in Green and Sustainable Chemistry*, *3*(August), 1–11. https://doi.org/10.1016/j.crgsc.2020.100016

Pawar, O., Deshpande, N., Dagade, S., Waghmode, S., & Nigam Joshi, P. (2016). Green synthesis of silver nanoparticles from purple acid phosphatase apoenzyme isolated from a new source Limonia acidissima. *Journal of Experimental Nanoscience*, *11*(1), 28–37. https://doi.org/10.1080/17458080.2015.1025300

Pham, Q. T., Huy, B. T., & Lee, Y. I. (2015). New highly efficient electrochemical synthesis of dispersed Ag2O particles in the vicinity of the cathode with controllable size and shape. *Journal of Materials Chemistry C*, *3*(29), 7720–7726. https://doi.org/10.1039/c5tc01274k

Rani, P., Kumar, V., Singh, P. P., Matharu, A. S., Zhang, W., Kim, K. H., Singh, J., & Rawat, M. (2020). Highly stable AgNPs prepared via a novel green approach for catalytic and photocatalytic removal of biological and

مجلة كلية التربية الاساسية
كلية التربية الاساسية – الجامعة المستنصرية
P- ISSN: 3007-3650 E- ISSN: 2706-8536
Journal of the College of Basic Education Vol.32 (No.137) 2026, pp.1110-1130

non-biological pollutants. *Environment International*, *143*, 1–13. https://doi.org/10.1016/j.envint.2020.105924

Rautela, A., Rani, J., & Debnath (Das), M. (2019). Green synthesis of silver nanoparticles from Tectona grandis seeds extract: characterization and mechanism of antimicrobial action on different microorganisms. *Journal of Analytical Science and Technology*, *10*(1), 1–10. https://doi.org/10.1186/s40543-018-0163-z

Roopan, S. M., Rohit, Madhumitha, G., Rahuman, A. A., Kamaraj, C., Bharathi, A., & Surendra, T. V. (2013). Low-cost and eco-friendly phyto-synthesis of silver nanoparticles using Cocos nucifera coir extract and its larvicidal activity. *Industrial Crops and Products*, *43*(1), 631–635. https://doi.org/10.1016/j.indcrop.2012.08.013

Saied, A. S., Gebauer, J., Hammer, K., & Buerkert, A. (2008). Ziziphus spina-christi (L.) Willd.: A multipurpose fruit tree. *Genetic Resources and Crop Evolution*, *55*(7), 929–937. https://doi.org/10.1007/s10722-007-9299-1

Shameran, J. S., Sewgil, S. A., & Awara, K. S. (2019). Biosynthesis of Silver Nanoparticles Extracted Using Proteus. *Journal of Engineering Sciences*, *2*(2), c1-c5. https://doi.org/10.21272/jes.2019.6(2).c1

Tanwar, K., & Joseph, D. (2025). Optical and Structural Studies of Silver Oxide Thin Films. *International Journal of Thin Film Science and Technology*, *14*(1), 57–62. https://doi.org/10.18576/ijtfst/140109

Theivasanthi, T., & Alagar, M. (2012). Electrolytic synthesis and characterization of silver nanopowder. *Nano Biomedicine and Engineering*, *4*(2), 58–65. https://doi.org/10.5101/nbe.v4i2.p58-65

Venkatachalam, P., Sangeetha, P., Geetha, N., & Sahi, S. V. (2015). Phytofabrication of Bioactive Molecules Encapsulated Metallic Silver Nanoparticles from Cucumis sativus L. and Its Enhanced Wound Healing Potential in Rat Model. *Journal of Nanomaterials*, *2015*, 1–9. https://doi.org/10.1155/2015/753193

Wei, S., Wang, Y., Tang, Z., Hu, J., Su, R., Lin, J., Zhou, T., Guo, H., Wang, N., & Xu, R. (2020). A size-controlled green synthesis of silver nanoparticles by using the berry extract ofSea Buckthornand their biological activities. *New Journal of Chemistry*, *44*(22), 9304–9312. https://doi.org/10.1039/d0nj01335h

Yagoub, A. E. A., Alshammari, G. M., Subash-Babu, P., Mohammed, M. A. A., Yahya, M. A., & Alhosain, A. I. (2021). Synthesis of ziziphus spina-christi (Jujube) root methanol extract loaded functionalized silver nanoparticle (ZS-Ag-NPs); physiochemical characterization and effect of ZS-Ag-NPs on adipocyte maturation, adipokine and vascular smooth muscle cell interactio. *Nanomaterials*, *11*(10), 1–20. https://doi.org/10.3390/nano11102563

Ziziphus, L., Ahmed, Z. F. R., Aldhanhani, A. R. H., Ahmed, Z. F. R., Tzortzakis, N., & Singh, Z. (2026). Maturity stage at harvest influences antioxidant phytochemicals and antibacterial activity of jujube fruit) Ziziphus mauritiana antibacterial activity of jujube fruit (Ziziphus mauritiana Lamk . and. *Annals of Agricultural Sciences*, *67*(2022), 196–203.

التخليق النباتي والدراسة التركيبية والبصرية لجسيمات Ag/Ag_2O النانوية باستخدام مزيج من مستخلص أوراق وثمار غير ناضجة للسدر العراقي(Christ's Thorn)

سندس هادي مرزا (1)

مجلة كلية التربية الاساسية
كلية التربية الاساسية – الجامعة المستنصرية
P- ISSN: 3007-3650 E- ISSN: 2706-8536
Journal of the College of Basic Education Vol.32 (No.137) 2026, pp.1110-1130

قسم الكيمياء، كلية التربية للعلوم الصرفة /ابن الهيثم، جامعة بغداد، العراق
(1)sundus.h.m@ihcoedu.uobaghdad.edu.iq
07707843740

مستخلص البحث:
تُقدم هذه الدراسة طريقةً جديدةً وصديقةً للبيئة وبسيطةً لتصنيع جسيمات نانوية من الفضة/أوكسيد الفضة (Ag/Ag_2O) باستخدام مزيج من مستخلص ثمار وأوراق نبات شوك المسيح العراقي غير الناضجة .(IF- LCT) تم التحقق من تحضير جسيمات الفضة النانوية بالعين المجردة، حيث تحول لون محلول نترات الفضة ($AgNO_3$) إلى اللون البني. أظهرت جسيمات Ag/Ag_2Oالنانوية رنينًا بلازمونيًا سطحيًا (SPR) عند 440 نانومتر. أُجريت لاحقًا دراسةٌ للخصائص باستخدام حيود الأشعة السينية(XRD) ، والأشعة فوق البنفسجية المرئية-(UV-Vis)، ومطيافية الأشعة تحت الحمراء بتحويل فورييه(FTIR) ، والمجهر الإلكتروني الماسح ذي الانبعاث الميداني(FE-SEM) ، ومطيافية تشتت طاقة الأشعة السينية (EDXS) وقد حُدد متوسط حجم البلورات لجسيمات Ag/Ag_2O النانوية، وفقًا لنتائج حيود الأشعة السينية، بـ 15.89 نانومتر. جميع المعاملات الأخرى اثبتت تُكون جسيمات نانوية من Ag/Ag_2O ذات نسبة عالية بين مساحة السطح والحجم، ونسبة تعبئة ذرية عالية(APF) ، ومساحة سطح نوعية عالية بشكل ملحوظ. أظهر تحليل المجهر الإلكتروني الماسح ذي الانبعاث الميداني (FE-SEM) أن جسيمات الفضة النانوية تتخذ شكلًا كرويًا وشبه كروي متكتلًا، بمتوسط حجم جسيمات يبلغ 21.65 نانومترًا. وأكد تحليل مطيافية تشتت طاقة الأشعة السينية (EDXS) أن الجسيمات النانوية تحتوي على الفضة والأكسجين. وكانت أفضل الظروف لتخليق جسيمات الفضة النانوية باستخدام مستخلص مائي بنسبة 1:10 إلى نترات الفضة عند درجة حرارة 25 درجة مئوية. وبلغت فجوة النطاق المباشر 2.96 إلكترون فولت. وأظهر تحليل طيف الأشعة تحت الحمراء (FTIR) امتدادًا مميزًا لحزم جسيمات Ag/Ag_2O النانوية المُحضرة. وتُشير النتائج المذكورة إلى نجاح تحضير جسيمات الفضة النانوية باستخدام مستخلص IF-LCT.

الكلمات المفتاحية: مساحة السطح النوعية، عامل الرص الذري، معادلة شيرر، جسيمات الفضة النانوية، مكعب ذو مركز وجهي.

ملاحظة: هل البحث مستل من رسالة ماجستير او اطروحة دكتوراه؟ نعم: كلا: √